Research article

Zejie Yu, Yang Ma and Xiankai Sun*

Photonic welding points for arbitrary on-chip optical interconnects

https://doi.org/10.1515/nanoph-2018-0078
Received June 27, 2018; revised August 27, 2018; accepted September 7, 2018

Abstract: Photonic integrated circuits (PICs) are an ideal platform for chip-scale computation and communication. To date, the integration density remains an outstanding problem that limits the further development of PIC-based photonic networks. Achieving low-loss waveguide routing with arbitrary configuration is crucial for both classical and quantum photonic applications. To manipulate light flows on a chip, the conventional wisdom relies on waveguide bends of large bending radii and adiabatic mode converters to avoid insertion losses from radiation leakage and modal mismatch, respectively. However, those structures usually occupy large footprints and thus reduce the integration density. To overcome this difficulty, this work presents a fundamentally new approach to turn light flows arbitrarily within an ultracompact footprint. A type of "photonic welding points" joining two waveguides of an arbitrary intersecting angle has been proposed and experimentally demonstrated. These devices with a footprint of less than 4 μm^2 can operate in the telecommunication band over a bandwidth of at least 140 nm with an insertion loss of less than 0.5 dB. Their fabrication is compatible with photonic foundry processes and does not introduce additional steps beyond those needed for the waveguides. Therefore, they are suitable for the mass production of PICs and will enhance the integration density to the next level.

Keywords: silicon photonics; optical interconnects; photonic integration; nanophotonic devices; inverse design

1 Introduction

Photonics is superior to electronics in the era of information technology. Photonic integrated circuits (PICs) have many significant advantages such as large bandwidth [1], low power consumption, high immunity to electromagnetic interference, and compatibility with quantum optical devices [2–6]. People have developed many high-performance on-chip applications such as optical interconnects [7], modulation [8], biosensing [9], quantum communication [2–6], and optomechanics [10]. However, as the complexity of on-chip optical interconnection continues to grow, a major issue in the development of PICs is the limited integration density, because the sizes of most photonic devices are tens of micrometers and on-chip interconnects also occupy a large area [11, 12]. Plasmonics, making use of materials such as Au, Ag, and TiN to break the diffraction limit [13], is one of the most used approaches to reduce the device footprints [14, 15], but the large ohmic loss of the plasmonic materials sets a limit to the propagation length of waveguides [16] and photon lifetime of cavities [17], yielding limited performance and applications of plasmonic circuits and devices. Besides using plasmonic materials, implementing structured photonic designs is also a route to reduce the footprint of photonic integrated devices. Photonic crystal waveguides, which guide the propagation of light with lateral confinement via the photonic bandgap effect, can make sharp turns of the propagation direction within an ultrasmall area [18–21]. However, the turning angle has limited choices because the guided light can only propagate along certain crystalline directions. Inverse design, which makes use of optimization algorithm, enables the search of structures in the entire space to achieve functionalities unexpected in a conventional design. The design method has been applied widely in multidisciplinary areas of science and engineering [22]. In integrated photonics, inverse-designed devices have been developed with ultracompact footprints that can be orders of magnitude smaller than those designed by conventional methods. For example, devices such as polarization rotators [23, 24], polarization beam splitters [25], mode demultiplexers [26, 27],

***Corresponding author: Xiankai Sun,** Department of Electronic Engineering, The Chinese University of Hong Kong, Shatin, New Territories, Hong Kong, e-mail: xksun@cuhk.edu.hk.
http://orcid.org/0000-0002-9137-0298
Zejie Yu and Yang Ma: Department of Electronic Engineering, The Chinese University of Hong Kong, Shatin, New Territories, Hong Kong

wavelength demultiplexers [28–30], power dividers [31, 32], reflectors [33], waveguide bends [34], and waveguide cloaking [35] have been demonstrated to have a footprint of only a few square micrometers.

Although much effort has been made to reduce the sizes of individual devices, reduction of the footprint of PIC interconnection is equally important and is yet to be demonstrated. Low-loss waveguide routing in PICs is crucial in both classical and quantum photonic applications to obtain high signal-to-noise ratios or to maintain the high fidelity of quantum states. To turn the direction of on-chip light flows, the conventional wisdom relies on waveguide bends of large bending radii and adiabatic mode converters, which avoid excessive insertion losses from the radiation leakage (bending loss) and the modal mismatch (scattering loss) [36], respectively. Those structures are known to occupy large footprints and thus reduce the integration density. Therefore, it is highly desired to find out an approach to turn the direction of light flows arbitrarily with negligible insertion loss within the smallest possible area. Here, we adopt the inverse design method to design photonic welding points, which are the photonic analog of electrical connections in integrated circuits, to join waveguides of arbitrary orientations within an extremely small area. Such photonic welding points have many distinct advantages. First, unlike the electrical welding points, which may introduce an additional insertion loss due to impedance mismatch for high-frequency signals, such photonic welding points are free from this problem and thus can be safely employed in PICs for high-frequency applications. Second, the structures are optimized only by engineering the shape of the borders, which can be described by a continuous and differentiable function. Such structures with gradually varying borders can be fabricated with high fidelity and also introduce minimal scattering loss to the transmitting light. Third, the fabrication process of the photonic welding points is CMOS compatible and requires only one step of lithography and etching. The designs are also highly robust with large fabrication tolerance, which guarantees the high performance for fabricated structures with deviation from the designed pattern.

2 Design procedure

In conventional wisdom, two waveguides can be joined by a waveguide bend to change the propagation direction of light, as shown in Figure 1A, where the gray part denotes SiO_2 and the purple part denotes silicon (Si). If the bend radius is not far greater than the light wavelength, the modal mismatch between the straight and bent waveguides and the poor confinement of the waveguide bend will introduce a significant insertion loss to light (Supporting Information). In addition, the waveguide bends of a small bend radius will also introduce a crosstalk between different optical modes [37].

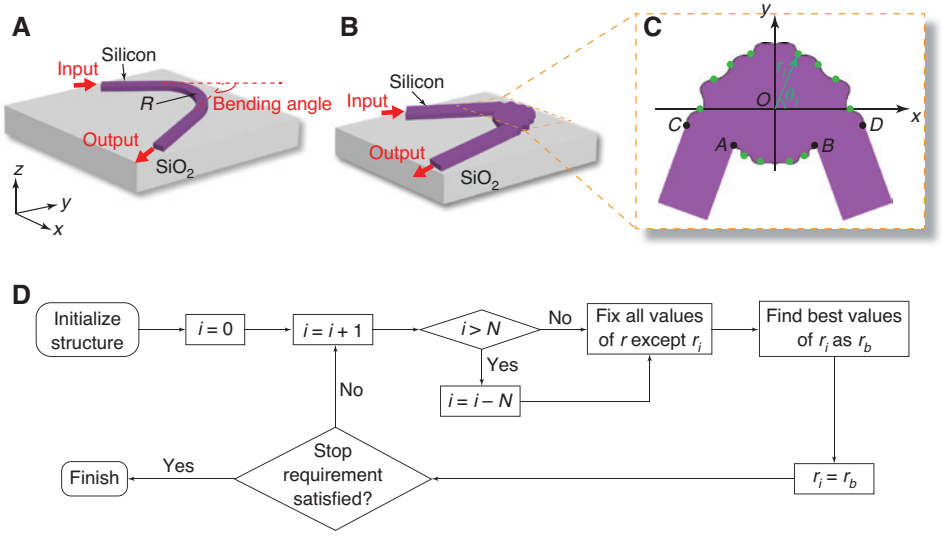

Figure 1: Conventional and new schemes for turning the direction of light flow on a chip.
(A) Schematic of the conventional waveguide bend for connecting two nonparallel waveguides. *R* is the inner radius of the waveguide bend, which should be at least tens of micrometers to avoid significant modal mismatch and bending loss. The gray and purple regions represent SiO_2 and Si, respectively. (B) Schematic of the photonic welding point for connecting two nonparallel waveguides. (C) Top view of the photonic welding point, the structure of which is defined by two continuous lines *AB* and *CD* going through the green dots. (D) Algorithm flowchart for the optimization process.

The photonic welding point realized within a small area, as shown in Figure 1B, is expected to connect waveguides with negligible insertion loss and crosstalk. We take the photonic welding point shown in Figure 1C as an example to explain the design process. The devices are designed on a silicon-on-insulator (SOI) platform with 220-nm Si layer on 3-μm buried oxide. We draw a small rectangle with an orange dashed line, as shown in Figure 1C, to indicate the design optimization region of the photonic welding point. Two continuous lines *AB* and *CD*, which are determined by the green discrete dots, delineate the borders of the photonic welding point structure, where the purple region denotes Si unetched and the white region denotes Si fully etched. The position of each discrete dot is described by the radial and angular coordinates (r_i and θ_i). The final r_i and θ_i are determined after several rounds of optimization.

As shown in Figure 1C, the structure of the photonic welding point is determined by two continuous lines *AB* and *CD*, which are fitted from the discrete 2*N* green dots by the triple spline interpolation. The distance between the adjacent dots is set larger than 100 nm to guarantee successful fabrication of the optimized structure. Due to the mirror symmetry of the structure with respect to the *y*-axis, we only need to optimize the positions of half of these

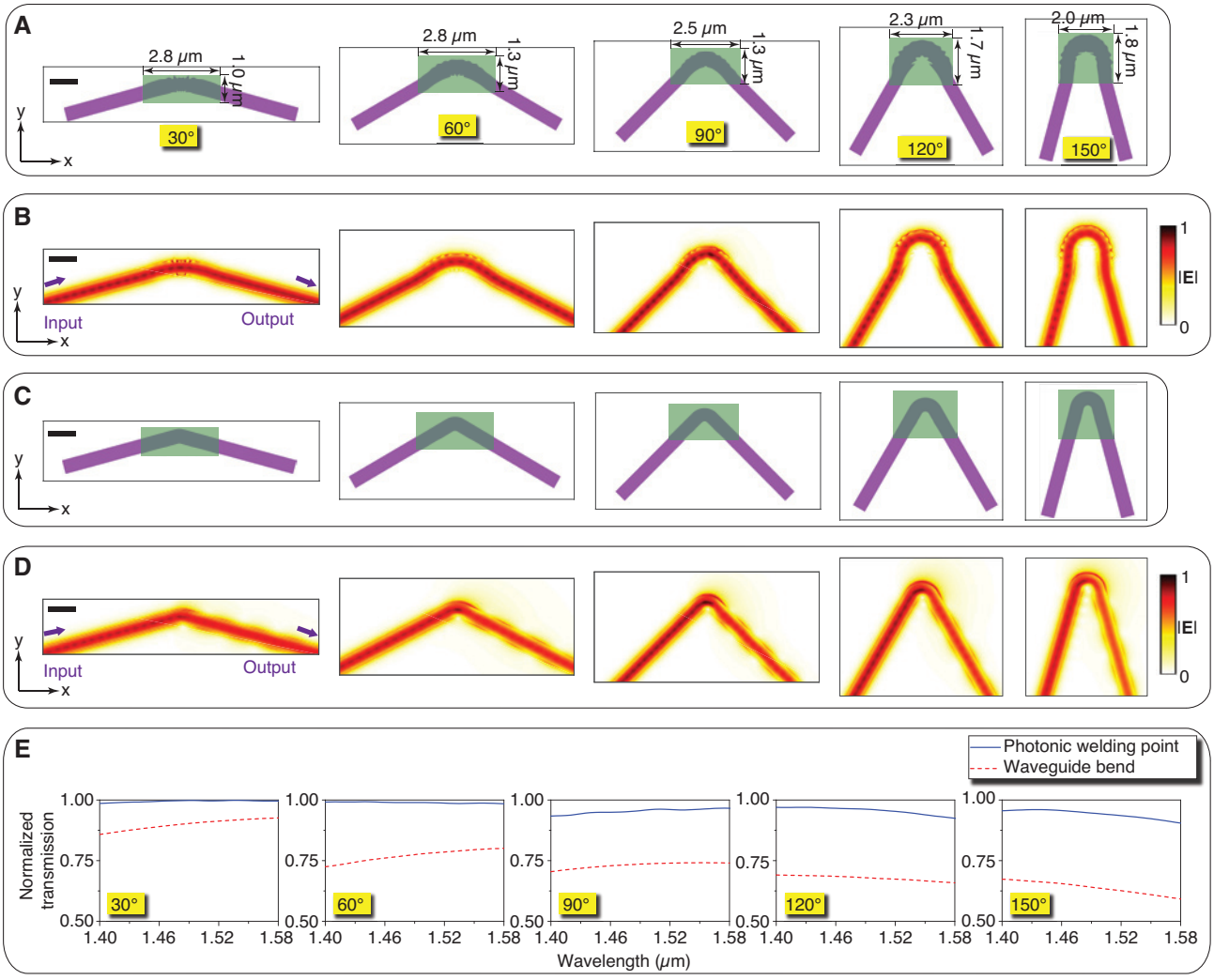

Figure 2: Designs and simulation results of the photonic welding points and waveguide bends.
(A) Optimized structures of photonic welding points connecting two waveguides with bending angles of 30°, 60°, 90°, 120°, and 150°. (B) Simulated electric field profiles of the TE_0 mode at 1.55 μm transmitting through the photonic welding points. (C) Schematic of waveguide bends connecting two waveguides with bending angles of 30°, 60°, 90°, 120°, and 150°. The inner radius of all waveguide bends is 0.15 μm. (D) Simulated electric field profiles of the TE_0 mode at 1.55 μm transmitting through the waveguide bends. The purple arrows indicate the light input and output directions. (E) Normalized transmission spectra of photonic welding points (blue solid lines) and waveguide bends (red dashed lines) connecting two waveguides with bending angles of 30°, 60°, 90°, 120°, and 150°. (A–D) Scale bars represent 1 μm.

discrete dots. During optimization, the four dots *A* to *D* are fixed, ensuring that the photonic welding point always connects with the two waveguides. The angular coordinates θ_i of the discrete dots are also fixed. The greedy optimization method (heuristic technique) was adopted to determine the radial coordinates r_i of the discrete dots. Figure 1D shows the algorithm flowchart for the optimization process. The figure of merit for the optimization is the normalized transmission of the fundamental transverse electric (TE_0) mode at 1.55 μm. We first generated a random value for each dot and then optimized them in series. During the serial optimization, we varied the individual r_i and restricted the dot within the orange dashed rectangle while fixing all the other dots. The temporary best r_i's were obtained after comparing the structural transmission of all attempted values. After several rounds of r_i optimization from the first dot to the last, we obtained the final structure of the photonic welding point when the insertion loss could not reduce in additional optimization runs. The above procedure was applied to obtain the photonic welding points for connecting waveguides with an arbitrary bending angle.

Without loss of generality, we designed the photonic welding points for connecting two 0.5-μm-wide waveguides with bending angles of 30°, 60°, 90°, 120°, and 150°. The structures for the additional representative bending angles can be found in the Supporting Information. Despite using the same procedure for design optimization, the computation time required to obtain the optimized photonic welding point for connecting waveguides with different bending angles varies. The structures for larger bending angles usually require a longer computation time. The five photonic welding points connecting waveguides with bending angles of 30°, 60°, 90°, 120°, and 150° took ~5 days in total using a normal 16-core desktop computer. Figure 2A shows the structures connected by the optimized photonic welding points in the green regions. Their zoomed-in views can be found in the Supporting Information. Figure 2B shows the simulated electric field |**E**| profiles of the TE_0 mode at 1.55 μm transmitting through the photonic welding points, which clearly indicate that light is confined tightly in the photonic welding points, thus avoiding the bending loss caused by small bend radii. The uniform intensity patterns in the output waveguide also prove no crosstalk introduced by the photonic welding points. Figure 2C shows the structures of conventional waveguide bends connecting the two waveguides, with an inner radius of the waveguide bend of 0.15 μm to maintain the same footprint of the corresponding photonic welding points. For light in the communication band around $\lambda = 1.55$ μm, the waveguide bend with an inner radius of ~$\lambda/10$ will inevitably introduce a large insertion loss due to the modal mismatch and sharp bending. Figure 2D shows the simulated electric field |**E**| profiles of the TE_0 mode at 1.55 μm transmitting through the waveguide bends, which clearly indicate the leakage of light from the waveguide bends. The intensity oscillation of light as seen in the output waveguide indicates that the light is not pure TE_0 mode anymore. Figure 2E shows the normalized spectra of transmission through the photonic welding points and waveguide bends, where the blue solid lines represent transmission from the photonic welding points and the red dashed lines represent transmission from the waveguide bends. A comparison between the blue solid and red dashed lines concludes that the waveguide bends will introduce significantly higher insertion loss, which is proportional to the bending angle, but the photonic welding points can avoid this loss and transport light from one waveguide to the other with any bending angle.

3 Experimental results and discussion

The devices of photonic welding points and waveguide bends were fabricated on an SOI wafer with 220-nm Si device layer on 3-μm buried oxide. The patterns of the devices were defined along with the input and output waveguides and grating couplers in a single step of electron-beam lithography with ZEP520A resist. Then, the patterns were transferred to the top Si layer by inductively coupled plasma reactive-ion etching with SF_6/C_4F_8 gas chemistry. The devices were finished after stripping the electron-beam resist and blow-drying.

Figure 3A (top) contains the optical microscope images of devices for characterizing the insertion loss of photonic welding points connecting waveguides with bending angles of 30°, 60°, 90°, 120°, and 150°, and Figure 3A (bottom) contains the corresponding scanning electron microscope (SEM) images zoomed in at the joint, all of which have a footprint of less than 4 μm^2. Figure 3B (top) contains the optical microscope images of devices for characterizing the insertion loss of waveguide bends connecting two waveguides with bending angles of 30°, 60°, 90°, 120°, and 150°, and Figure 3B (bottom) contains the SEM images zoomed in at the joint. We included multiple photonic welding points or waveguide bends in each device to reduce the measurement error as the insertion loss of a single photonic welding point is intrinsically small. On-chip integrated grating couplers were employed for coupling light between the on-chip waveguides and optical fibers, because grating couplers can work not only

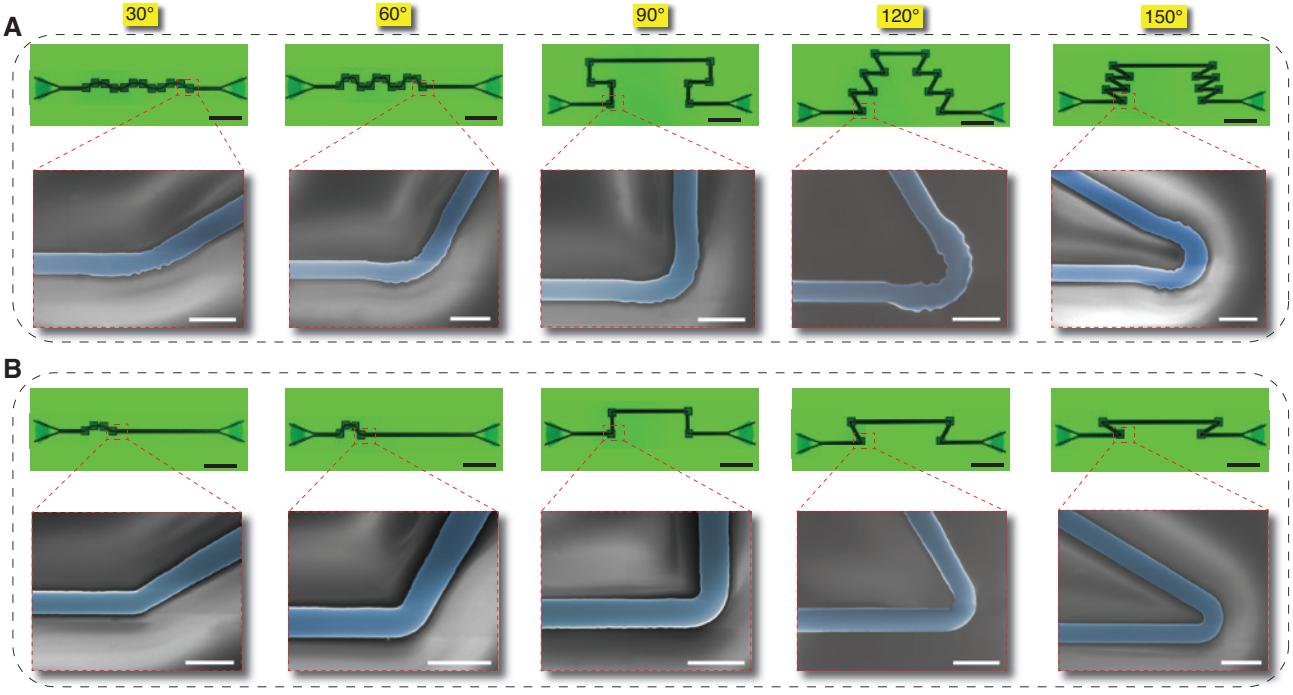

Figure 3: Device images of the photonic welding points and waveguide bends.
(A) Optical microscope and SEM images of the fabricated devices for measuring the transmission loss of photonic welding points connecting two waveguides with bending angles of 30°, 60°, 90°, 120°, and 150°. The devices with bending angles of 30°, 60°, 120°, and 150° each contain 12 photonic welding points, whereas the one with bending angle of 90° contains 8 photonic welding points. (B) Optical microscope and SEM images of the fabricated devices for measuring the transmission loss of waveguide bends connecting two waveguides with bending angles of 30°, 60°, 90°, 120°, and 150°. Each device contains four cascaded bends for reducing the measurement error. Scale bars represent 40 μm in all optical microscope images and 1 μm in all SEM images.

as a power coupler but also as a mode filter to select the desired TE_0 mode for the on-chip waveguides. Devices that consist of a pair of grating couplers connected directly with a straight waveguide were fabricated in the same run to calibrate the insertion loss introduced by the grating couplers. We also fabricated multiple devices of photonic welding points and waveguide bends with grating couplers covering different operating bands to overcome the limitation of narrow operating bandwidth of grating couplers.

The fabricated devices were characterized by spectroscopic measurement of their optical transmission. Light from a tunable semiconductor laser (wavelength 1440–1580 nm) was sent over a single-mode fiber, with the polarization state adjusted by a fiber polarization controller, into the device under test via the input grating coupler. The transmitted light coupled out of the output grating coupler was collected by a photodetector. Figure 4 plots the normalized transmission spectra of a single photonic welding point and a single waveguide bend, where the simulation for the fabricated structure was conducted by importing the device's SEM image into Lumerical and neglecting the roughness along the out-of-plane direction. It is clear that the three spectra (measured, simulated for the ideal, and simulated for the fabricated) agree with each other. The insertion loss of the photonic welding points all maintains less than 0.5 dB in the entire wavelength range of 1440–1580 nm, whereas that of the waveguide bends increases with the bending angle and can reach up to 3.0 dB.

Due to the uncontrollable imperfection in nanofabrication, the sizes of fabricated devices can often have tens of nanometers deviation from the original design due to, for example, the over/underexposure in the lithography process or over/underetch in the dry etching. Therefore, fabrication tolerance is an important characteristic for assessing the performance of devices. Here, we simulated the transmission of the photonic welding points with size variation of $\Delta w = \pm 40$ nm as shown in Figure 5A, and the results are plotted in Figure 5B for structures with bending angles of 30°, 60°, 90°, 120°, and 150°. The normalized transmission spectra of the ideal structure and the structures with $\Delta w = 40$ and -40 nm clearly indicate that the photonic welding points preserve a similar performance

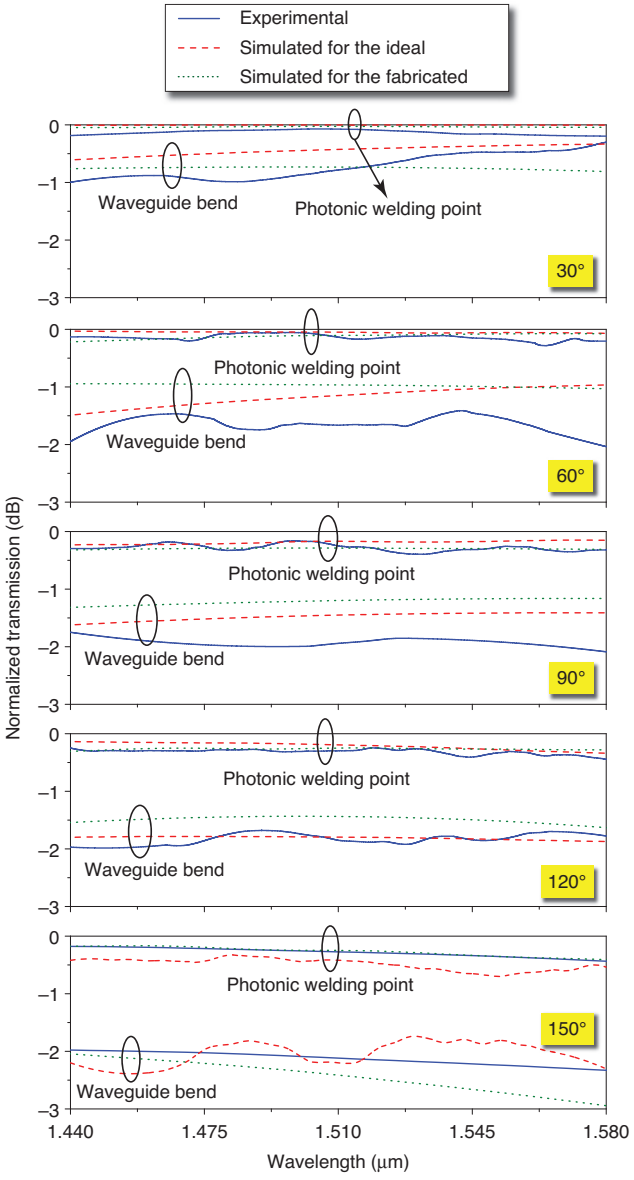

Figure 4: Experimental and simulated normalized transmission spectra of single photonic welding point and waveguide bend for connecting two waveguides with bending angles of 30°, 60°, 90°, 120°, and 150°.
Blue solid lines represent the experimentally measured results, red dashed lines represent the simulated results for the ideal structure, and green dotted lines represent the simulated results for the fabricated structure.

under the size variation of $\Delta w = \pm 40$ nm, which is within typical fabrication errors of the actual device fabrication. The fundamental reason for such a large fabrication tolerance is that an overall change of the positions of all the individual dots r_i that define the borders of the photonic welding point does not introduce much transmission variation.

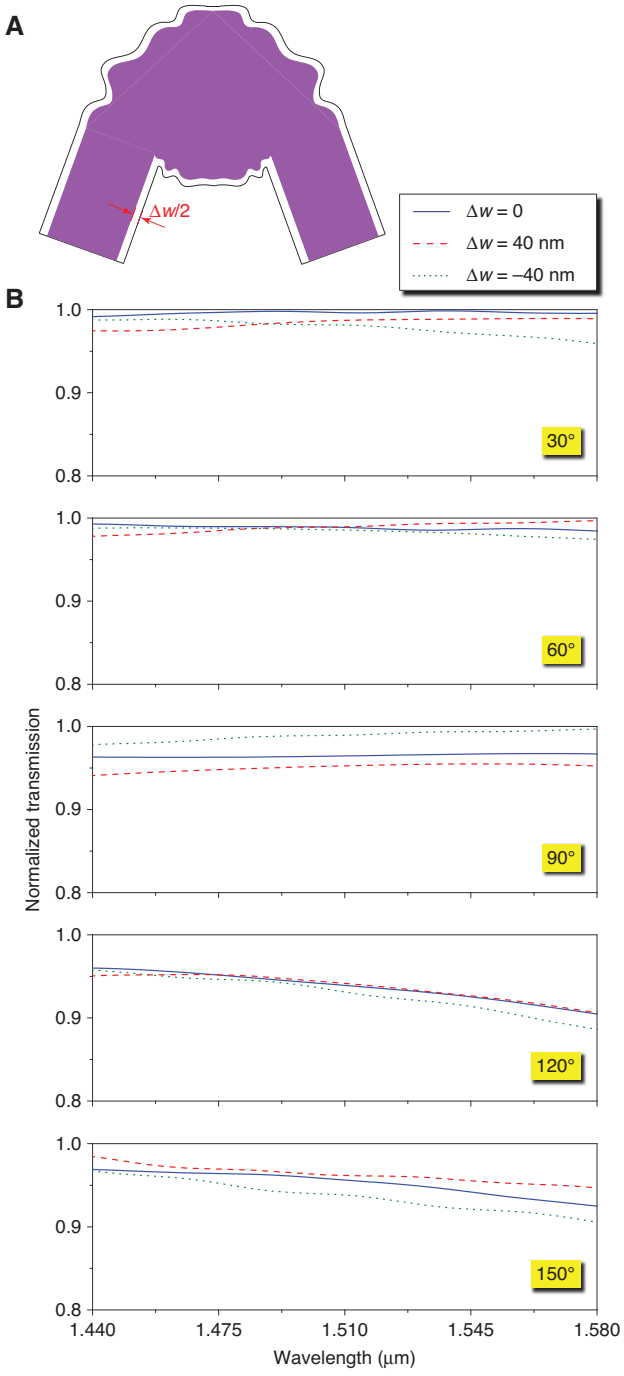

Figure 5: Fabrication tolerance analysis.
(A) Illustration of a typical fabrication error of photonic welding points. The purple area denotes the fabricated structure, whereas the black solid line denotes the border of the original design. The width of the fabricated structure may have a deviation Δw from the designed value. (B) Analysis of the fabrication deviation in photonic welding points for connecting two waveguides with bending angles of 30°, 60°, 90°, 120°, and 150°. Blue solid, red dashed, and green dotted lines represent the ideal structure, the structure with width deviation $\Delta w = 40$ nm, and the structure with width deviation $\Delta w = -40$ nm, respectively.

4 Conclusion

In conclusion, we have designed and demonstrated experimentally a new type of structures, namely the "photonic welding points", for connecting two waveguides with an arbitrary bending angle on a chip. The feature sizes of these photonic welding points are about two orders of magnitude smaller than conventional waveguide bends. The designed devices have large fabrication tolerance, and the fabrication process is simple and straightforward, which involves only a single step of electron-beam lithography with subsequent dry etching on an SOI wafer. The insertion loss from both simulation and measurement results keeps below 0.5 dB in the wavelength range of 1440–1580 nm. Therefore, our proposed photonic welding points can be employed as a standard module in PICs for boosting the density of photonic integration to the next level.

Acknowledgments: This work was supported by the Early Career Scheme (Project No. 24208915) and the General Research Fund (Project No. 14208717) sponsored by the Research Grants Council of Hong Kong and by the NSFC/RGC Joint Research Scheme (Project No. N_CUHK415/15) sponsored by the Research Grants Council of Hong Kong and the National Natural Science Foundation of China.

References

[1] Zhang C, Zhang S, Peters JD, Bowers JE. $8\times8\times40$ Gbps fully integrated silicon photonic network on chip. Optica 2016;3:785–6.
[2] Sibson P, Kennard JE, Stanisic S, Erven C, O'Brien JL, Thompson MG. Integrated silicon photonics for high-speed quantum key distribution. Optica 2017;4:172–7.
[3] Silverstone JW, Bonneau D, Ohira K, et al. On-chip quantum interference between silicon photon-pair sources. Nat Photonics 2013;8:104–8.
[4] Politi A, Matthews JCF, Thompson MG, Brien JLO. Integrated quantum photonics. IEEE J Sel Top Quantum Electron 2009;15:1673–84.
[5] Kues M, Reimer C, Roztocki P, et al. On-chip generation of high-dimensional entangled quantum states and their coherent control. Nature 2017;546:622–6.
[6] Politi A, Cryan MJ, Rarity JG, Yu S, O'Brien JL. Silica-on-silicon waveguide quantum circuits. Science 2008;320:646–9.
[7] Dai D, Bowers JE. Silicon-based on-chip multiplexing technologies and devices for Peta-bit optical interconnects. Nanophotonics 2014;3:283–311.
[8] Liu A, Jones R, Liao L, et al. A high-speed silicon optical modulator based on a metal-oxide-semiconductor capacitor. Nature 2004;427:615–8.
[9] Estevez MC, Alvarez M, Lechuga LM. Integrated optical devices for lab-on-a-chip biosensing applications. Laser Photon Rev 2012;6:463–87.
[10] Sun X, Xu K, Tang HX. Monolithically integrated, ultrahigh-frequency cavity nano-optoelectromechanical system with on-chip germanium waveguide photodetector. Opt Lett 2014;39:2514–7.
[11] Li G, Yao J, Thacker H, et al. Ultralow-loss, high-density SOI optical waveguide routing for macrochip interconnects. Opt Express 2012;20:12035–9.
[12] Sun X, Liu H-C, Yariv A. Adiabaticity criterion and the shortest adiabatic mode transformer in a coupled-waveguide system. Opt Lett 2009;34:280–2.
[13] Gramotnev DK, Bozhevolnyi SI. Plasmonics beyond the diffraction limit. Nat Photonics 2010;4:83–91.
[14] Melikyan A, Alloatti L, Muslija A, et al. High-speed plasmonic phase modulators. Nat Photonics 2014;8:229–33.
[15] Haffner C, Heni W, Fedoryshyn Y, et al. All-plasmonic Mach-Zehnder modulator enabling optical high-speed communication at the microscale. Nat Photonics 2015;9:525–8.
[16] Zhu BQ, Tsang HK. High coupling efficiency silicon waveguide to metal-insulator-metal waveguide mode converter. J Lightwave Technol 2016;34:2467–72.
[17] Chu H-S, Bai P, Li E-P, Hoefer WRJ. Hybrid dielectric-loaded plasmonic waveguide-based power splitter and ring resonator: compact size and high optical performance for nanophotonic circuits. Plasmonics 2011;6:591–7.
[18] Frandsen LH, Harpøth A, Borel PI, Kristensen M, Jensen JS, Sigmund O. Broadband photonic crystal waveguide 60° bend obtained utilizing topology optimization. Opt Express 2004;12:5916–21.
[19] Lin S-Y, Chow E, Hietala V, Villeneuve PR, Joannopoulos JD. Experimental demonstration of guiding and bending of electromagnetic waves in a photonic crystal. Science 1998;282:274–6.
[20] Mekis A, Chen JC, Kurland I, Fan S, Villeneuve PR, Joannopoulos JD. High transmission through sharp bends in photonic crystal waveguides. Phys Rev Lett 1996;77:3787–90.
[21] Borel PI, Harpøth A, Frandsen LH, Kristensen M, Shi P, Jensen JS, Sigmund O. Topology optimization and fabrication of photonic crystal structures. Opt Express 2004;12:1996–2001.
[22] Bendsoe M, Sigmund O. Topology optimization: theory, methods and applications. Berlin, Springer, 2003.
[23] Yu Z, Cui H, Sun X. Genetic-algorithm-optimized wideband on-chip polarization rotator with an ultrasmall footprint. Opt Lett 2017;42:3093–6.
[24] Majumder A, Shen B, Polson R, Menon R. Ultra-compact polarization rotation in integrated silicon photonics using digital metamaterials. Opt Express 2017;25:19721–31.
[25] Shen B, Wang P, Polson R, Menon R. An integrated-nanophotonics polarization beamsplitter with 2.4×2.4 μm^2 footprint. Nat Photonics 2015;9:378–82.
[26] Piggott AY, Lu J, Lagoudakis KG, Petykiewicz J, Babinec TM, Vučković J. Inverse design and demonstration of a compact and broadband on-chip wavelength demultiplexer. Nat Photonics 2015;9:374–7.
[27] Chang W, Lu L, Ren X, et al. Ultra-compact mode (de) multiplexer based on subwavelength asymmetric Y-junction. Opt Express 2018;26:8162–70.
[28] Frellsen LF, Ding Y, Sigmund O, Frandsen LH. Topology optimized mode multiplexing in silicon-on-insulator photonic wire waveguides. Opt Express 2016;24:16866–73.

[29] Su L, Piggott AY, Sapra NV, Petykiewicz J, Vučković J. Inverse design and demonstration of a compact on-chip narrowband three-channel wavelength demultiplexer. ACS Photonics 2018;5:301–5.
[30] Borel PI, Bilenberg B, Frandsen LH, et al. Imprinted silicon-based nanophotonics. Opt Express 2007;15:1261–6.
[31] Mak JCC, Sideris C, Jeong J, Hajimiri A, Poon JKS. Binary particle swarm optimized 2×2 power splitters in a standard foundry silicon photonic platform. Opt Lett 2016;41:3868–71.
[32] Xu K, Liu L, Wen X, et al. Integrated photonic power divider with arbitrary power ratios. Opt Lett 2017;42:855–8.
[33] Yu Z, Cui H, Sun X. Genetically optimized on-chip wideband ultracompact reflectors and Fabry-Perot cavities. Photonics Res 2017;5:B15–9.
[34] Shen B, Polson R, Menon R. Metamaterial-waveguide bends with effective bend radius $<\lambda_0/2$. Opt Lett 2015;40:5750–3.
[35] Shen B, Polson R, Menon R. Increasing the density of passive photonic-integrated circuits via nanophotonic cloaking. Nat Commun 2016;7:13126.
[36] Vlasov YA, McNab SJ. Losses in single-mode silicon-on-insulator strip waveguides and bends. Opt Express 2004;12:1622–31.
[37] Wang J, Zhao C, Wei B, et al. Measurement of the intermodal crosstalk of a bent multimode waveguide. Appl Opt 2016;55:7619–23.

Supplementary Material: The online version of this article offers supplementary material (https://doi.org/10.1515/nanoph-2018-0078).